PAPER

An Optimum Design of Error Diffusion Filters Using the Blue Noise in All Graylevels

Junghyeun HWANG[†a)], ***Student Member***, **Hisakazu KIKUCHI**[†b)], ***Fellow***, **Shogo MURAMATSU**[†], ***Member***, ***and*** **Jaeho SHIN**[††], ***Nonmember***

SUMMARY The error diffusion filter in this paper is optimized with respect to the ideal blue noise pattern corresponding to a single tone level. The filter coefficients are optimized by the minimization of the squared error norm between the Fourier power spectra of the resulting halftone and the blue noise pattern. During the process of optimization, the binary pattern power spectrum matching algorithm is applied with the aid of a new blue noise model. The number of the optimum filters is equal to that of different tones. The visual fidelity of the bilevel halftones generated by the error diffusion filters is evaluated in terms of a weighted signal-to-noise ratio, Fourier power spectra, and others. Experimental results have demonstrated that the proposed filter set generates satisfactory bilevel halftones of grayscale images.

key words: *digital halftoning, error diffusion, blue noise, power spectrum, binary pattern power spectrum matching*

1. Introduction

Digital halftoning methods [1]–[18] can make a significant difference in printed or displayed image quality. Halftone images resemble the original continuous-tone images, when viewed from a distance due to the low-pass filtering nature of the human visual system (HVS) [13]–[16], [19]–[22]. Digital halftoning is used to render a continuous-tone image on printers, computer monitors or other displaying devices that are capable of producing a few levels of tone. The perceptual quality of the halftoned image depends on the spatial distribution of the bilevel dots. The error diffusion algorithms [1]–[9] among various halftoning techniques [10]–[18] have been proposed for realizing the homogeneous dot distribution and sharp rendering of bilevel images.

It is known that error diffusion halftoning produces unwanted textures such as worm artifacts at highlight and shadow regions and banding effects at mid-tone regions. Banding effects can strongly appear at so-called key levels [4], [8]. They are basically defined by multiples of the reciprocals of small integers, if the continuous-tone resides in the interval of [0, 1].

The error diffusion halftoning presented by Ostromoukhov in [8] is attractive among many algorithms. In spite of low complexity, it produces fine bilevel halftones where banding and worm artifacts are significantly suppressed. One of the reasons for its state-of-the-art performance is the optimal design of error diffusion filters. The coefficients of the error diffusion filters were designed at several extended key levels by minimizing the error between the Fourier power spectra [23] of the targeted halftone and a blue noise pattern. As for graylevels different from the key levels, the filters were defined by a linear interpolation between two coefficients for the neighboring key levels.

However, the optimality is not always ensured for a two-dimensional error diffusion filter of which coefficients are defined by linear interpolation. In addition, the power spectrum of the ideal blue noise has been implicitly described in [8] rather than explicitly: error diffusion halftoning was suggested for generating blue noise patterns. That is, the ideal bilevel patterns used for the design are lack of a proof of the true blue noise properties.

In this paper, such a short-cut is avoided, and a straightforward optimization at every graylevel is developed for a possible improvement. A new blue noise model is also given for better solutions in the optimization. Real blue noise patterns [9]–[12], [24]–[26] are actually constructed via the binary pattern power spectrum matching (BIPPSM) algorithm [14], [27], [28], before they are applied to the optimization of error diffusion filters. The proposed method produces comparable visual quality of bilevel halftones and better power spectral characteristics than those in Ref. [8]. The tone-adaptive control of the filter coefficients is simple and fast; it is enough to read out an entry in a linear coefficient array of which entry is indexed by the graylevel expressed in digital count.

This paper is organized as follows. After a brief analysis of the error diffusion algorithm, a characterization of blue noise is given in Sect. 2. A half of Sect. 3 is devoted to the construction of blue noise patterns by the BIPPSM algorithm, and is followed by a description of the optimum design of a set of error diffusion filters. Experimental results are given in Sect. 4. Visual fidelity of the halftone images produced by the error diffusion filters is investigated in terms of a weighted signal-to-noise ratio, Fourier power spectrum, radially averaged power spectral density, pair correlation, and others. Conclusions follow in Sect. 5.

Manuscript received November 9, 2009.
Manuscript revised April 6, 2010.

[†]The authors are with the Department of Electrical and Electronic Engineering, Niigata University, Niigata-shi, 950-2181 Japan.

[††]The author is with the Department of Electronics Engineering, Dongguk University, 3-26 Pil-dong, Jung-gu, Seoul 100-715, Korea.

a) E-mail: hwang@telecom0.eng.niigata-u.ac.jp

b) E-mail: kikuchi@eng.niigata-u.ac.jp

DOI: 10.1587/transfun.E93.A.1465

2. Error Diffusion Halftoning

2.1 A Description of the Error Diffusion Algorithm

The continuous-tone input and the bilevel output are assumed as $x(m,n) \in [0,1]$ and $y(m,n) \in \{0,1\}$, where m and n stand for the horizontal and vertical locations, respectively. The error diffusion halftoning shown in Fig. 1 is expressed by the following equation system.

$$a(m,n) = x(m,n) + \sum_{k,\ell \in \Omega} w_{k,\ell}^{(i)} d(m-k, n-\ell) \tag{1}$$

$$y(m,n) = \lfloor a(m,n) + 0.5 \rfloor \tag{2}$$

$$d(m,n) = a(m,n) - y(m,n) \tag{3}$$

where $\lfloor \cdot \rfloor$ represents the maximum integer that does not exceed the argument. Ω stands for the neighborhood where the quantization error is diffused. $w_{k,\ell}^{(i)}$ denotes a coefficient of the error diffusion filter for the ith level in the tone intensity. The error diffusion filter has three coefficients in this work. The error is diffused at the east, southwest, and south locations with respect to the location of the target pixel being quantized at present. Pixels are visited in serpentine scanning to reduce the chance of worm patterning.

The behavior of error diffusion can be analyzed in the frequency domain. To do that, the quantization is represented by a linear stochastic model shown in Fig. 2, where $e(m,n) \in (-0.5, 0.5]$ is a random variable with an independent[†] uniform distribution, and represents the quantization error. Applying the quantization model to Eq. (2) and applying the two-dimensional z-transform to Eqs. (1)–(3), one obtains

$$A(z_1,z_2) = X(z_1,z_2) + W^{(i)}(z_1,z_2)D(z_1,z_2) \tag{4}$$

$$Y(z_1,z_2) = A(z_1,z_2) + E(z_1,z_2) \tag{5}$$

$$D(z_1,z_2) = A(z_1,z_2) - Y(z_1,z_2). \tag{6}$$

The augmented input and the diffusion signal, A and D, are eliminated to obtain

$$Y = X + \left(1 - W^{(i)}\right) E. \tag{7}$$

It is found that the low frequency components of the quantization error are swept out to high frequencies [2], as far as the the error diffusion filter is a lowpass filter and is of unity-gain at $z_1 = z_2 = 1$. This implies that

$$w_{1,0}^{(i)} + w_{-1,1}^{(i)} + w_{0,1}^{(i)} = 1. \tag{8}$$

Since $1 - W^{(i)}$ is a two-dimensional highpass filter, error diffusion halftones posses a blue noise-like characteristic by the second term in the right-hand side of Eq. (7). Also, $1 - W^{(i)}$ takes different gains depending on the spatial directions. As a result, banding artifacts at key levels can be induced at mid-tone areas, if the area is uniform and large enough to trigger locking to regular and stable patterning [4]. In the highlight and shadow areas, since the probability of the minority pixels is very low, the direction-dependent delivery of the quantization error can be visible as the worm textures, where a few bilevel dots align with a particular orientation. The worm patterning effect is weak in the case of serpentine scanning, because the error diffusion directions are alternated along the horizontal direction line by line.

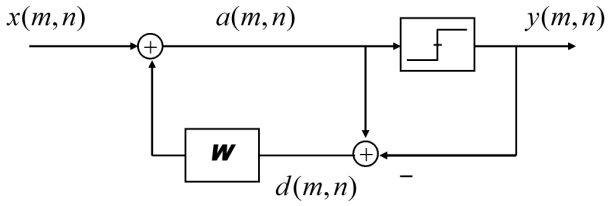

Fig. 1 Error diffusion halftoning.

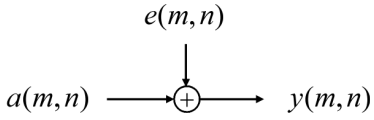

Fig. 2 Linear stochastic model for the uniform quantization.

2.2 Characterization of Blue Noise

A uniform bilevel image of which graylevel is $g \in [0,1]$ on average is considered. Pixels are assumed to be located on the rectangular sampling grids of which spacing is S[††]. In the ideal blue noise pattern, the average sample distance between two minority pixels is characterized by the principal wavelength [10], [11] defined by

$$\lambda(g) = S / \sqrt{\min(g,\ 1-g)} \tag{9}$$

where $\min(\cdots)$ denotes the minimum in the entries. Note that the minority pixels are distributed as uniform as possible, while the probability with respect to a minority pixel such that no more minority pixels are found within a distance of $\lambda(g)$ is high unlike the white noise.

The blue noise is also characterized by the radially averaged power spectral density[†††] (RAPSD) [10]–[12], [14] as a function of the radial frequency, f_r. The principal frequency [10], [11] defined by

[†]The quantization error in bilevel halftoning is actually input signal-dependent [3], [4]. However, the issue is still an open problem [2], because the quantization is a deterministic process governed by a strong nonlinearity.

[††]Without loss of generality, S is assumed to be one for displaying a digital image on regular rectangular grids.

[†††]When the baseband in the horizontal and vertical frequencies is divided into a sequence of annuli centered at the origin with different radii, each annulus covers a set of frequency grids. The set is written by $\rho(f_r)$ and the number of elements in $\rho(f_r)$ is denoted by $N(\rho(f_r))$. The RAPSD of a signal $x(m,n)$ is defined by

$$X_r^2(f_r) = \frac{1}{N(\rho(f_r))} \sum_{(k,\ell) \in \rho(f_r)} |X(k,\ell)|^2$$

where $X(k,\ell)$ is the DFT of $x(m,n)$.

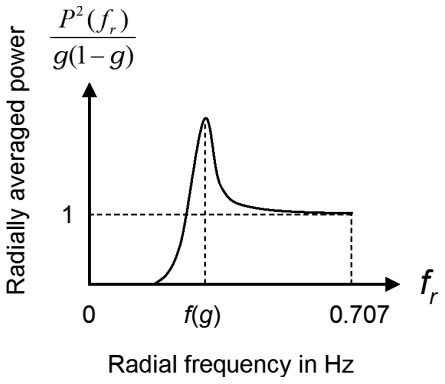

Fig. 3 RAPSD of a typical blue noise pattern.

$$f(g) = 1/\lambda(g) \tag{10}$$

plays an important role. The RAPSD of a blue noise pattern has a peak at $f_r = f(g)$ as illustrated in Fig. 3. It shows a rapid attenuation as the radial frequency decreases from $f(g)$, and is zero at $f_r = 0$. It approaches a fixed value of 1 in the frequencies above $f(g)$. The unity-level at high frequencies owes to the normalization by $g(1-g)$ [10], [11] that is the variance of the white noise pattern of which graylevel is g.

The radially symmetric cut-off property in the two-dimensional power spectrum is also a consequence of the basic characteristics. Visually-pleasing bilevel patterns are desirable to acquire these features, which is one of the topics in the following section.

3. Design of the Error Diffusion Filters

3.1 Design of Blue Noise Patterns

Mitsa and Parker [27] presented the BIPPSM algorithm to make a bilevel blue noise pattern. Starting from a given bilevel white noise pattern, the bilevel pattern is updated to reach a blue noise pattern by a sequence of iterative procedures.

***B1*:** Compute the discrete Fourier transform (DFT) of the present bilevel pattern. Define the spectral shaping profile by dividing the RAPSD of the ideal blue noise by that of the bilevel pattern.

***B2*:** The radial extension of the RAPSD shaping profile is multiplied with the DFT of the latest bilevel pattern, and is followed by the inverse DFT to create a continuous-tone image that has been modified to mimic the desirable blue noise.

***B3*:** The difference between the continuous-tone image and the latest bilevel pattern is computed pixel by pixel.

***B4*:** According to the order of error magnitude, zero and one which have the largest error in each ranking are swapped on their locations.

***B5*:** When the mean square error between the latest and previous zero/one-swapped patterns is smaller than that in the previous iteration, the above steps are repeated.

Otherwise, the algorithm is terminated.

In summary, the resulting bilevel pattern gains the spectral features of a desirable blue noise by its radial extension onto the 2-dimensional DFT domain. It also acquires the desirable minimum-distance limit property among minority pixels by swapping of pairs of zero and one.

Based on the characterizations of the blue noise in the previous section, a graphical user interface (GUI) has been developed to implement BIPPSM algorithm in MATLAB. The algorithm is however time-consuming and the peaking at $f(g)$ is also missing in the RAPSD of an ideal blue noise in BIPPSMA [14], [27]. To overcome the weakness, the ideal RAPSD model for the blue noise is given by

$$\frac{P(f_r)}{\sqrt{g(1-g)}} = \begin{cases} \gamma_1\left(e^{f_r} - 1\right) & \text{for } f_r \le f_g \\ \gamma_2\left(e^{-\left(f_r - \frac{1}{\sqrt{2}}\right)} - 1\right) + 1 & \text{for } f_r \ge f_g \end{cases} \tag{11}$$

where

$$\gamma_1 = \frac{h}{e^{f_g} - 1} \tag{12}$$

$$\gamma_2 = \frac{h-1}{e^{-\left(f_g - \frac{1}{\sqrt{2}}\right)} - 1} \tag{13}$$

and $f_g = f(g)$. h stands for the peak height and its value is derived from an assumption of power conservation between the blue noise model and the ideal white noise pattern:

$$\int_0^{\frac{1}{\sqrt{2}}} \frac{P^2(f_r)}{g(1-g)} df_r = \frac{1}{\sqrt{2}}. \tag{14}$$

The solution is given in Appendix A. While the principal frequency is scaled down by $\sqrt{2}$ in Ref. [27], such an experimental remedy is unnecessary owing to the theoretical peaking built in Eq. (11).

3.2 Optimum Design of Error Diffusion Filters

Every error diffusion filter is designed for a different graylevel. The goal is to obtain a set of error diffusion filters every of which generates a bilevel halftone showing the blue noise characteristics, when a continuous-tone image of a specific graylevel is halftoned by using the filter. Possible guidelines for obtaining satisfactory filters are summarized into the following three points.

***C1*:** The RAPSD of a blue noise pattern satisfies the three characteristics presented in Sect. 2.2 as illustrated in Fig. 3; peaking at $f(g)$, rapid decay in low frequencies, and asymptotic convergence to the unity-level at high frequencies[†].

***C2*:** The Fourier power spectrum of a blue noise pattern is

[†]When an RAPSD matters, "high" and "low" frequencies are mentioned with reference to the principal frequency.

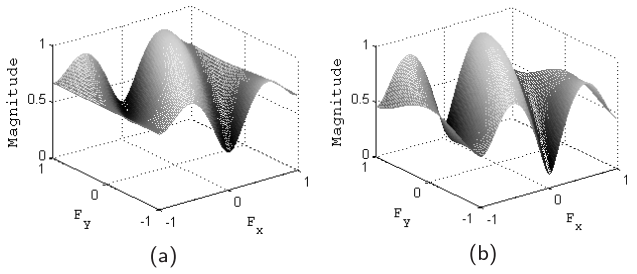

Fig. 4 Frequency responses of error diffusion filters for the graylevel of 80/255. (a) Ostromoukhov and (b) proposed.

radially symmetric, and shows a highpass characteristic of which cut-off frequency is slightly lower than $f(g)$.

***C3*:** With respect to any minority pixel, the probability such that no more minority pixels are found within a distance of $\lambda(g)$ is high.

The guideline *C1* is the most basic property of the blue noise, and it is responsible for the desirable 2-dimensional DFT profile by the radial extension. Hence the guideline *C2* is effective and enough during the optimization, as far as *C1* is reflected in the DFT profile. The guideline *C3* is implicitly taken into account in the optimization through the blue noise reference pattern designed by the method in Sect. 3.1. It is worth to note that *C3* is expectable from the intrinsic nature of error diffusion that divides the quantization error into different pieces to scatter them around different locations.

Since the error diffusion filters should be identical for dark levels and light levels in the sense of minority pixels, we impose the condition that

$$\mathbf{W}^{(i)} = \mathbf{W}^{(255-i)} \tag{15}$$

where

$$\mathbf{W}^{(i)} = \left(w^{(i)}_{1,0},\, w^{(i)}_{-1,1},\, w^{(i)}_{0,1}\right). \tag{16}$$

$\mathbf{W}^{(i)}$ is a vector notation for the coefficients of the error diffusion filter. The superscript in parentheses denotes the graylevel in 8-bit digital count.

The filter coefficients are optimized by minimizing the error between the power spectra of the generated error diffusion-halftone and the blue noise pattern via simulated annealing [29], [30]. The minimization of the filter coefficients for the ith graylevel is expressed by

$$\mathbf{W}^{(i)} = \arg\min_{\mathbf{W}^{(i)}} \{\|Y(\mathbf{W}^{(i)}) - B^{(i)}\|\} \tag{17}$$

where $Y(\mathbf{W}^{(i)})$ is the DFT of the bilevel halftone produced by the error diffusion and $B^{(i)}$ is that of the blue noise pattern of the ith level, which has been obtained in the previous subsection. $\|\cdot\|$ stands for the L_2 norm.

The initial values of filter coefficients are set as $\mathbf{W}^{(i)} = \left(\frac{2}{4}, \frac{1}{4}, \frac{1}{4}\right)$. A 1024×1024-pixel uniform patch is used in course of the optimizations for individual tones.

The coefficient values obtained by the proposed optimum design are presented in Appendix B. As an example, the frequency responses of Ostromoukhov's filter and the filter designed for the graylevel $g = 80/255$ are shown in parts (a) and (b) in Fig. 4, respectively. Since the former is a result of coefficients interpolation between two key levels of $77/255^{\dagger}$ and $85/255$, these frequency responses are a little bit different.

4. Experimental Results

The design of bilevel blue noise patterns is evaluated before comparing halftone images, because the bilevel patterns provide the critical reference for the optimization of error diffusion filters.

4.1 Design Validation of Bilevel Blue Noise Patterns

The design of a bilevel blue noise pattern is checked by several objective measures. Figure 5(a) is a design example of such a bilevel pattern. Since its graylevel is $g = 227/255$, $\lambda(g) \simeq 3.0$ and $f(g) \simeq 0.33$. As seen in the bilevel pattern and a magnified view in part (b), there are fewer minority pixels within a distance shorter than $\lambda(g)$.

The spatial statistics are also checked by means of *pair correlation*[††] of which definition is given in the literature [14]. The pair correlation is the occurrence frequencies of the same sort pixels, with respect to every minority pixel, in the annuli with different radii. If the pair correlation value is small at a distance, any more minority pixels are expectable to be absent around individual minority pixels at that distance. A desirable pair correlation in the blue noise patterns is hence close to zero below the principal wavelength. The fact is evident in the pair correlation in part (c), where its value rapidly vanishes as the radial distance decreases below $\lambda(g) = 3.0$. On the other hand, the pair correlation is constant above $\lambda(g)$. It is an evidence of a homogeneous distribution with respect to distance between minority pixels.

In the Fourier power spectrum shown in part (d), higher intensities are plotted in lighter and the circle indicates the equi-distant frequencies at $f_r = f(g)$. The radial symmetry is observed to be satisfactory. No abnormal intensities corresponding to unwanted spatially-periodic textures are found. Favorable properties in RAPSD are seen in part (e), where peaking around $f_r = 0.33$ is apparent.

Isotropy validation in the bilevel pattern is checked by *anisotropy* [10], [11] in the radial frequency domain and *directional distribution* [14] in the spatial domain. Anisotropy is defined by the relative variance of the DFT components within different annuli to the RAPSD. If the anisotropy of a

[†]The tone level 77 in digital count is not a key level in nature. However it is treated as one of 30 key levels in total in Ref. [8] as well as 107, 95, 72 and others. This is because they are empirically problematic.

[††]Pair correlation is dissimilar to the correlation between continuous-tone pixels such as auto-correlation. The pair correlation represents the degree of popularity of the pairs of the same sort pixels between "black" and "white."

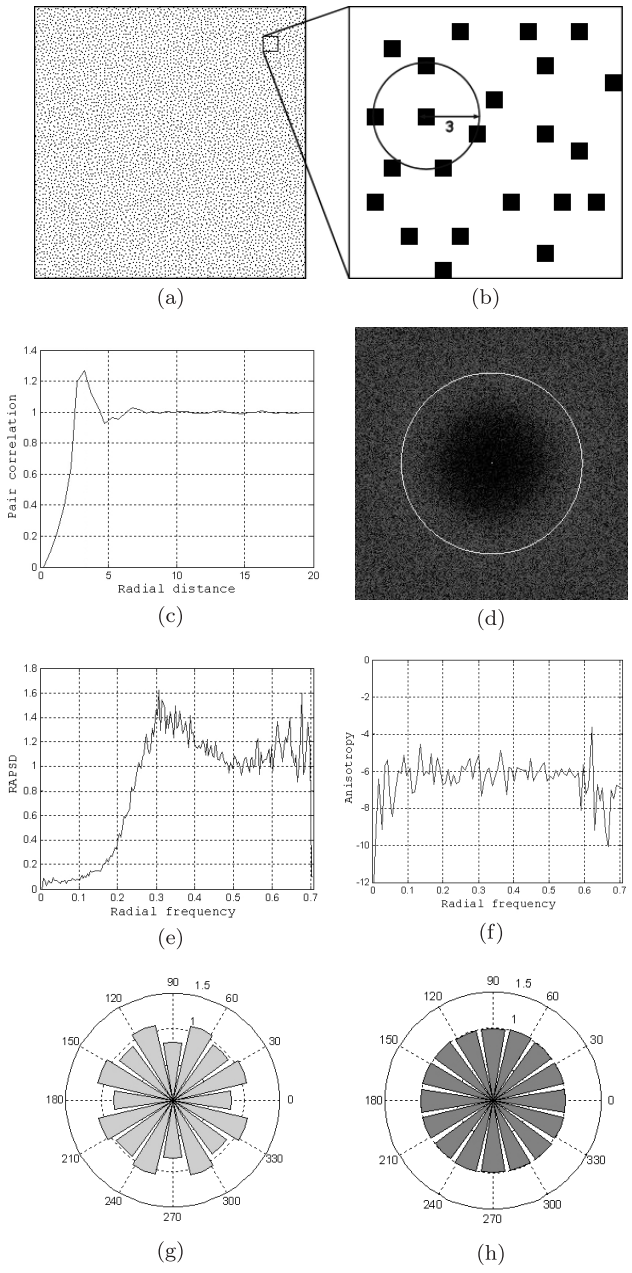

Fig. 5 A design example of a blue noise pattern. (a) blue noise pattern of the graylevel at 227 in 8-bit digital count, (b) magnified view of a part, (c) pair correlation, (d) Fourier power spectrum, (e) RAPSD, (f) anisotropy, (g) near range directional distribution, and (h) far range directional distribution.

bilevel pattern is low and flat over the radial frequencies, the pattern is said to be isotropic. It is evident that the anisotropy in part (f) is at the levels around −6 dB and indicates fine isotropy.

Directional distribution is a measure of near and far distributions of bilevel dots. It is defined by the occurrence frequencies in fan-shaped directional sections of a few annuli specified by different radii[†]. The near and far directional distributions in different directions are shown in parts (g) and (h), where the radial length from the origin represents the

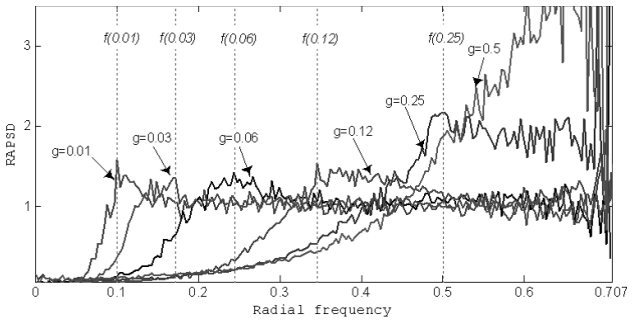

Fig. 6 Radial averaged power spectra of some blue noise patterns designed by using the BIPPSM-incorporated GUI.

value of directional distribution. The near and far ranges are meant by the distances shorter than $2\lambda(g)$ in between minority pixels and those between $2\lambda(g)$ and $4\lambda(g)$, respectively. It is observed that the near directional distributions have the values around 0.8 to 1.1 and far ones are perfect, showing that the pattern is tolerably isotropic.

Some RAPSDs of designed blue noise patterns are plotted in Fig. 6, where vertical dashed lines indicate the locations of individual principal frequencies. The asymptotic approach to the unity-gain at the highest radial frequency is observed except for the case of $f(g) = \frac{1}{\sqrt{2}}$ which will show a peaking instead of the asymptotic convergence.

4.2 Comparisons of Halftone Images

The performance of the proposed error diffusion is evaluated in comparison to two representative error diffusion algorithms in Refs. [1], [8]. The evaluation measures include visual inspections, Fourier power spectrum, RAPSD, pair correlation, and a weighted signal-to-noise ratio (WSNR) [21], [22]. WSNR is defined by

$$\mathrm{WSNR} = 10\log_{10}\frac{255^2}{\mathrm{WMSE}} \tag{18}$$

where

$$\mathrm{WMSE} = \frac{1}{MN}\sum_{m=0}^{M-1}\sum_{n=0}^{N-1} V(m,n) \times |X(m,n) - Y(m,n)|^2. \tag{19}$$

$V(m,n)$ is a visual weight derived from the contrast sensitivity function [22]. $X(m,n)$ represents the DFT of an $M \times N$-pixel continuous-tone image, and $Y(m,n)$ is the DFT of the bilevel halftone image.

The first experiments are on a comparison among three types of error diffusion of a grayscale ramp image of

[†]Since each section is defined by two radii, r_1 and r_2, and an angle θ, with a fixed angular step, say $\pi/8$, the directional distribution is written by $D(r_1, r_2, \theta)$, where $r_1 < r_2$. $D(0, r_1, \theta)$ and $D(r_1, r_2, \theta)$ are referred to as the near range and far range distribution, respectively. If the value of a directional distribution is larger or smaller than one, the population of minority pixels is too many or too few, respectively.

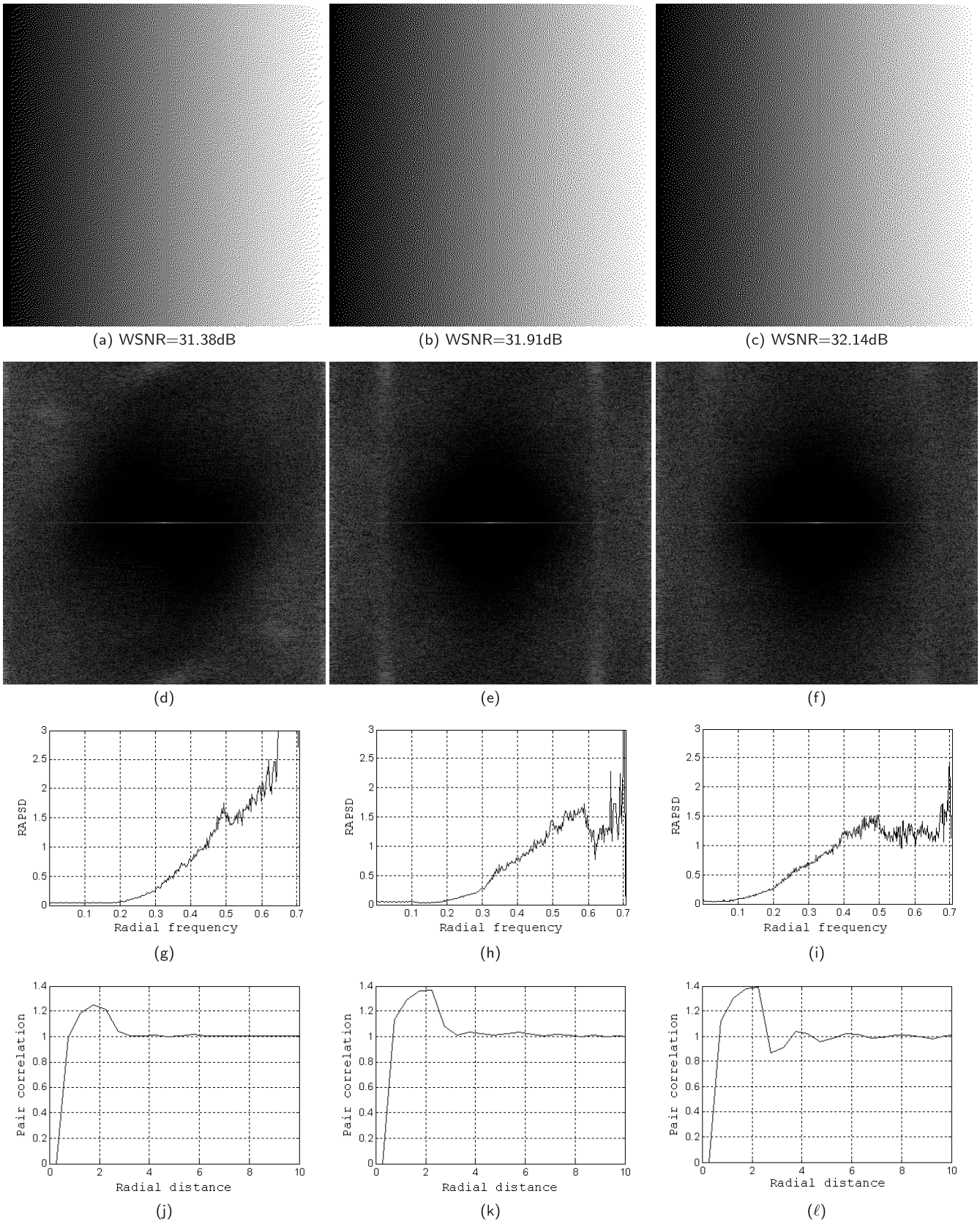

Fig. 7 Results of different error diffusion halftoning algorithms applied to a grayscale ramp. Three columns from left to right show the results by Floyd-Steinberg, Ostromoukhov, and the proposed methods, respectively. (a), (b), and (c) in the top row are the halftones. (d), (e), and (f) in the second row are Fourier power spectra. (g), (h), and (i) in the third row are RAPSDs. (j), (k), and (ℓ) in the bottom row are pair correlations.

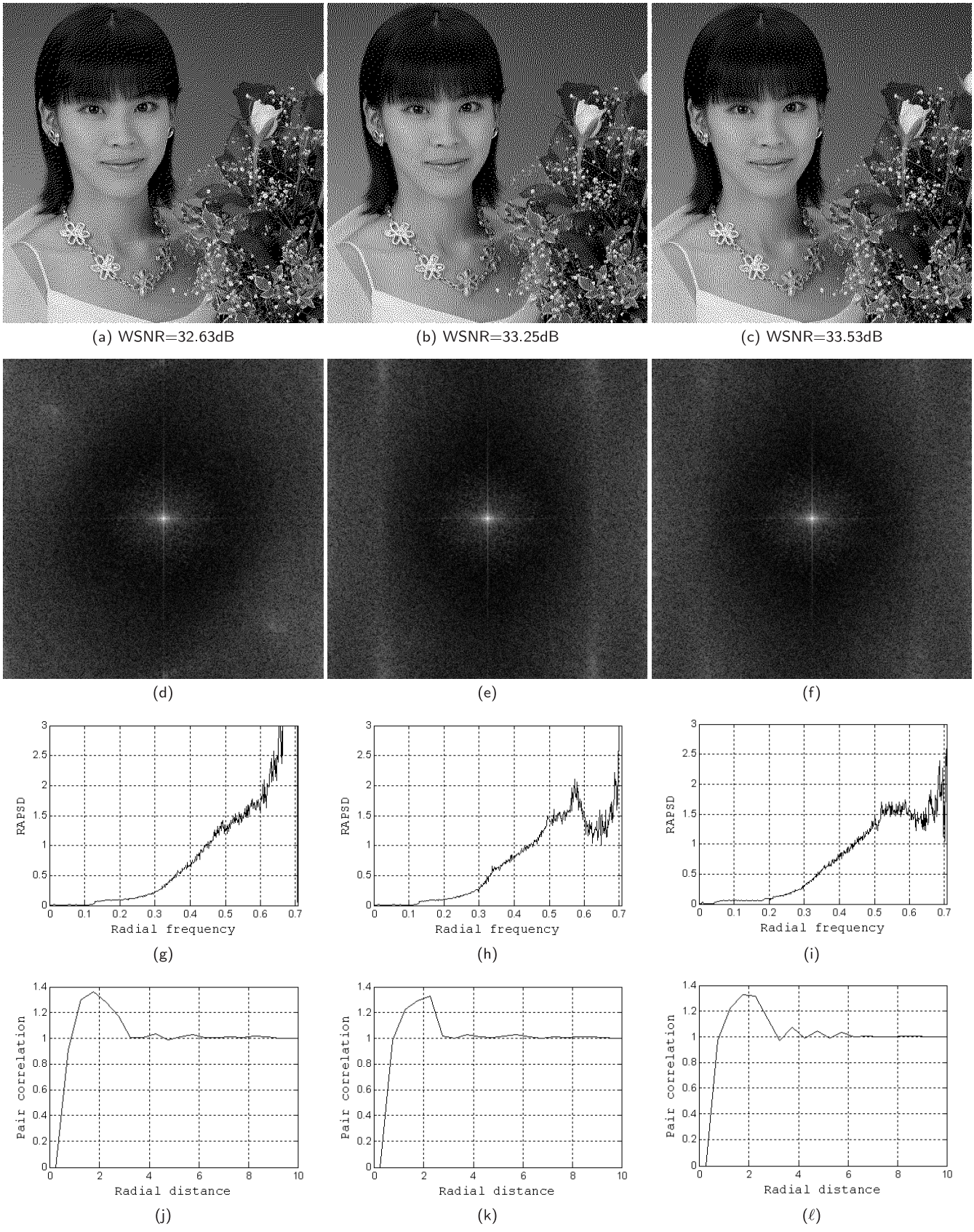

Fig. 8 Results of different error diffusion halftoning algorithms applied to *Portrait*. Three columns from left to right show the results by Floyd-Steinberg, Ostromoukhov, and the proposed methods, respectively. (a), (b), and (c) in the top row are the halftones. (d), (e), and (f) in the second row are Fourier power spectra. (g), (h), and (i) in the third row are RAPSDs. (j), (k), and (ℓ) in the bottom row are pair correlations.

512×512 pixels. Obtained bilevel halftones, Fourier power spectra, RAPSDs, and pair correlations are shown in Fig. 7, where left-to-right three columns correspond to those of Floyd-Steinberg [1], Ostromoukhov [8], and the proposed method, respectively. The bilevel halftones are shown in parts (a), (b), and (c) on the top row, where WSNR values are given. Among them, part (c) shows less artificial patterning and is more visually-pleasing.

Parts (d), (e), and (f) show the 2-dimensional plots of the Fourier spectra of the resultant halftones, where stronger components are displayed in lighter. The horizontal line across the origin shows the image content corresponding to the horizontal gradation of the ramp. The other components are the quantization errors caused by halftoning. A directional bias is observed in part (d). Two vertical distributions around ±0.5 Hz in the horizontal frequency in part (e) have been considerably suppressed in part (f).

Clear differences are observed in RAPSD as found in parts (g), (h), and (i) on the third row in Fig. 7. Since the average principal frequency of the ramp image is calculated as $\bar{f}_g = \int_0^{0.5} \sqrt{g}\, dg + \int_{0.5}^{1} \sqrt{1-g}\, dg \simeq 0.47$, the RAPSD in part (i) is found to have the desirable radial cut-off response around $f_r = \bar{f}_g$. On the other hand, the RAPSD peak in part (h) is located around $f_r = 0.59$, and (g) shows an excessive growth in high frequencies. It is evident that a comprehensive distribution of radial frequency components in part (i) is closer to the blue noise characteristics than that in part (g) and (h).

The pair correlation statistics are shown in parts (j), (k), and (ℓ). In part (j), the peak is located around the radial distance of 1.8, which is shorter than $\bar{\lambda}_g = 1/\bar{f}_g = 2.1$. Both of the pair correlations in parts (k) and (ℓ) are satisfactory.

The error diffusion bilevel halftoning has been applied to a natural image, *Portrait_1X*[†], and the results are shown in Fig. 8. Parts (a), (b), and (c) are parts of the halftone images. The WSNR values are 32.63, 33.25, and 33.53 in dB in the cases of Floyd-Steinberg, Ostromoukhov, and the proposed, respectively. Banding artifacts are visually observed in the area at the top-left behind the head in part (a), while they are considerably suppressed in part (c). The power spectra shown in parts (d), (e), and (f) are similar to those in Fig. 7; a directional bias in part (d), vertical distributions in part (e), and improved radial symmetry in part (f). It implies that the high-frequency noise involved with the proposed halftoning is closer to the blue noise than those produced by the other two schemes.

Since RAPSD and pair correlation are statistical measures and since the target image in this experiment is a natural image with a variety of variations, precise comparisons on these statistics are more or less significant. In spite of the complex situation, a few remarks can be drawn regarding RAPSDs and pair correlations on the bottom two rows in Fig. 8. Note that the average principal frequency and average principal wavelength of the test image are calculated as $\bar{f}_g = 0.52$ and $\bar{\lambda}_g = 1.9$, respectively. As for RAPSD, no peaking at $\bar{f}_g$ is observed in part (g), and the peak location in part (h) is higher than $\bar{f}_g = 0.52$, while the peak in (i) is identical to $\bar{f}_g$. The pair correlations in parts (j) and (ℓ) are fine showing a peak at 1.9 in radial distance, but the peak location in part (k) is farther than $\bar{\lambda}_g$. The overall behaviors of these measures obtained by the proposed method mimic the blue noise characteristics better than those by the other two methods.

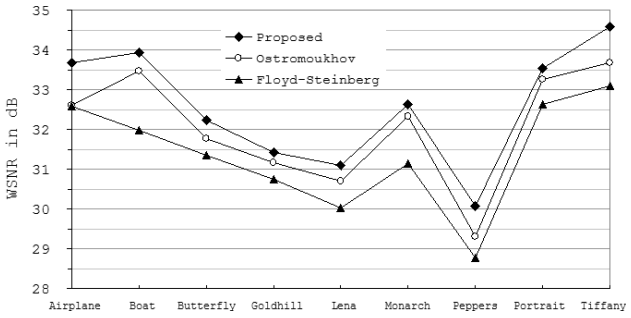

Fig. 9 WSNR on grayscale images produced by three methods of Floyd-Steinberg, Ostromoukhov, and the proposed.

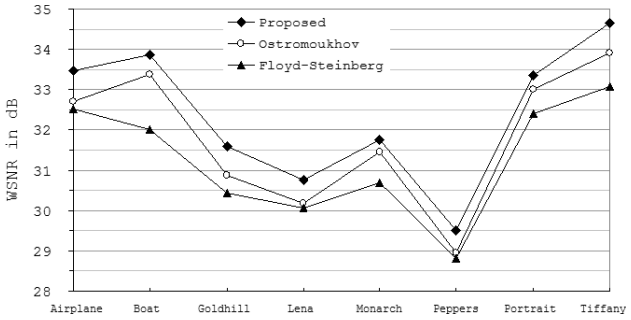

Fig. 10 Average WSNRs in the case of 24-bit color images.

Visual fidelity in terms of WSNR is experimented on 8-bit grayscale images of *Airplane*, *Boat*, *Butterfly*[††], *Goldhill*, *Lena*, *Monarch*, *Peppers*, *Portrait_1X*, and *Tiffany*. The grayscale data is the luma defined by ITU-R BT.601 [31]. WSNR values are plotted in Fig. 9, where the proposed bilevel halftoning outperforms the other two methods.

As for 24-bit RGB color images, the proposed error diffusion halftoning has been separately applied to three color components. The WSNRs have been averaged over three components. The result is shown in Fig. 10. It is seen that the performances are very similar to those in the case of grayscale images. No objectionable textures that are color-specific have been detected by on-display visual inspections.

5. Conclusions

We have presented an extension of the error diffusion halftoning in Ref. [8]. Bilevel blue noise patterns have been actually generated by BIPPSM algorithm combined with a new RAPSD model of blue noise. A set of error diffusion filters have been optimized for individual blue noise patterns

[†]http://www.colour.org/tc8-04/test_images/Sony/

[††]Courtesy of Victor Ostromoukhov

with different tone intensities. The visual fidelity has been tested by means of several objective measures. The bilevel halftones produced by the proposed error diffusion halftoning are more favorable than those by two typical error diffusions that have been experimented in this work.

More in-depth investigations are necessary for color error diffusion halftoning for printing, because many aspects[†] should be taken into account to reduce unwanted effects unique to color digital halftoning [13], [14], [16].

Acknowledgments

The authors thank Professor Daniel Leo Lau of University of Kentucky for comments and discussions on an earlier BIPPSM program code of this work. Also, the authors would like to thank anonymous reviewers and the associate editor for their helpful comments for improving the presentation of this paper.

References

[1] R. Floyd and L. Steinberg, "An adaptive algorithm for spatial gray scale," Soc. for Information Display Symp. Digest of Technical Papers, pp.36–37, 1975.
[2] D. Anastassiou, "Error diffusion coding for A/D conversion," IEEE Trans. Circuits Syst., vol.36, no.9, pp.1175–1186, 1989.
[3] K.T. Knox and R. Eschbach, "Threshold modulation in error diffusion," J. Electronic Imaging, vol.2, no.3, pp.185–192, July 1993.
[4] K.T. Knox, "Evolution of error diffusion," J. Electronic Imaging, vol.8, no.4, pp.422–429, 1999.
[5] J.H. Kim, T.I. Chung, H.S. Kim, and K.S. Son, "New edge-enhanced error diffusion algorithm based on the error sum criterion," J. Electronic Imaging, vol.4, no.2, pp.172–178, April 1995.
[6] K.E. Spaulding, D.W. Couwenhoven, and R.L. Miller, "Improved error diffusion algorithm incorporating a visual model," in Recent Progress in Digital Halftoning II, ed. R. Eschbach, pp.58–66, IS&T, 1999.
[7] P. Li and J.P. Allebach, "Tone dependent error diffusion," Proc. SPIE, vol.4663, pp.310–321, Jan. 2002.
[8] V. Ostromoukhov, "A simple and efficient error-diffusion algorithm," Proc. SIGGRAPH 2001, vol.9, pp.567–572, Aug. 2001.
[9] P.M. Jodoin and V. Ostromoukhov, "Error-diffusion with blue-noise properties for midtones," Proc. SPIE, vol.4663, pp.293–301, 2002.
[10] R. Ulichney, Digital Halftoning, MIT Press, Cambridge, Massachusetts, 1987.
[11] R.A. Ulichney, "Dithering with blue noise," Proc. IEEE, vol.76, no.1, pp.56–79, Jan. 1988.
[12] R. Ulichney, "A review of halftoning techniques," SPIE, vol.3963, pp.378–391, 2000.
[13] H.R. Kang, Digital Color Halftoning, SPIE Press and IEEE Press, Bellingham, 1999.
[14] D.L. Lau and G.R. Arce, Modern Digital Halftoning, 2nd ed., CRC Press, New York, 2008.
[15] M. Mese and P.P. Vaidyanathan, "Recent advances in digital halftoning and inverse halftoning methods," IEEE Trans. Circuits Syst. I, Fundam. Theory Appl., vol.49, no.6, pp.790–805, June 2002.
[16] F.A. Baqai, J.H. Lee, A.U. Agar, and J.P. Allebach, "Digital color halftoning," IEEE Signal Process. Mag., vol.22, no.1, pp.87–96, 2005.
[17] M. Mese and P.P. Vaidyanathan, "Image halftoning and inverse halftoning for optimized dot diffusion," IEEE Int. Conf. on Image Processing, vol.2, pp.54–58, Oct. 1998.
[18] M.R. Gupta and J.J. Bowen, "Ranked dither for high-quality robust printing," J. Opt. Soc. America A, vol.25, no.6, pp.1454–1458, June 2008.
[19] J. Sullivan, R. Miller, and G. Pios, "Image halftoning using a visual model in error diffusion," J. Opt. Soc. America A, vol.10, no.8, pp.1714–1724, Aug. 1993.
[20] J. Sullivan, L. Ray, and R. Miller, "Design of minimum visual modulation halftone patterns," IEEE Trans. Syst. Man Cybern., vol.21, no.1, pp.33–38, Jan. 1991.
[21] J.L. Mannos and D.J. Sakrison, "The effects of a visual fidelity criterion on the encoding of images," IEEE Trans. Inf. Theory, vol.IT-10, no.4, pp.525–535, 1974.
[22] T. Mitsa and K.L. Varkur, "Evaluation of contrast sensitivity functions for the formulation of quality measures incorporated in halftoning algorithms," IEEE Int. Conf. Acoust., Speech Signal Process., vol.5, pp.301–304, 1993.
[23] D. Kermisch and P.G. Roetling, "Fourier spectrum of halftone images," in Selected Papers on Digital Halftoning, SPIE Milestone Series, ed. J.P. Allebach, vol.MS 154, pp.3–10, 1999.
[24] D.L. Lau, R. Ulichney, and G.R. Arce, "Blue and green noise halftoning models," IEEE Signal Process. Mag., vol.20, no.4, pp.28–38, July 2003.
[25] K.J. Parker, "Blue noise mask overview," Tech. Rep., Reserch Corporation Technologies, May 2006.
[26] K.J. Parker and T. Mitsa, "Method and appartus for halftone rendering of a gray scale image using a blue noise mask," US Patent, no.5 111 310, May 1992.
[27] T. Mitsa and K.J. Parker, "Digital halftoning technique using a blue noise mask," J. Opt. Soc. America A, vol.9, no.11, pp.1920–1929, Nov. 1992.
[28] M. Yao and K.J. Parker, "Modified approach to the construction of a blue noise mask," J. Electronic Imaging, vol.3, no.1, pp.92–97, 1994.
[29] W.H. Press, S.A. Teukoisky, W.T. Vettering, and B.P. Flannery, Numerical Recipes in C, 2nd ed., Cambridge University Press, New York, 1992.
[30] S.P. Banks, Signal Processing, Image Processing and Pattern Recognition, Prentice Hall, 1990.
[31] Rec. ITU-R BT.601-6, Studio encoding parameters of digital television for standard 4:3 and wide-screen 16:9 aspect ratios, ITU, 2007.

Appendix A: The Solution of Eq. (14)

Substituting Eq. (11) to Eq. (14) and carrying out the integration, one obtains a quadratic equation with respect to h as follows.

$$a(h-1)^2 + 2b(h-1) + c = 0 \qquad (A\cdot 1)$$

where

$$a = 1 - \frac{1}{d_1} + \frac{f_g}{d_1^2} - \frac{1}{d_2} + \frac{f_h}{d_2^2}$$

$$b = \frac{3}{2} - \frac{1}{d_1} + \frac{f_g}{d_1^2} - \frac{f_h}{d_2}$$

$$c = \frac{1}{2} - \frac{1}{d_1} + \frac{f_g}{d_1^2} - f_g$$

$$d_1 = e^{f_g} - 1$$

$$d_2 = e^{f_h} - 1$$

[†]They include dot arrangement between dot-on-dot or dot-off-dot, dot profile, dot gain, device profile, and tone/color reproductions. Most of them could be investigated if a target printing system would be well defined.

Table A· 1 Coefficients of the Error Diffusion Filters. The index i stands for the graylevel in 8-bit digital count. Note that $w^{(i)}_{0,1} = 1 - w^{(i)}_{1,0} - w^{(i)}_{-1,1}$.

i	$w^{(i)}_{1,0}$	$w^{(i)}_{-1,1}$	i	$w^{(i)}_{1,0}$	$w^{(i)}_{-1,1}$
0	0.5333	0.2000	64	0.5058	0.4909
1	0.6957	0.1739	65	0.4884	0.4913
2	0.6591	0.1591	66	0.4718	0.4919
3	0.6286	0.1429	67	0.4538	0.4960
4	0.5938	0.1250	68	0.4353	0.4941
5	0.5854	0.1463	69	0.4184	0.4974
6	0.5714	0.1667	70	0.4016	0.4980
7	0.5833	0.1667	71	0.3844	0.5000
8	0.5610	0.1951	72	0.3668	0.5019
9	0.5625	0.2125	73	0.3941	0.4529
10	0.5488	0.2317	74	0.4269	0.4011
11	0.5444	0.2453	75	0.4538	0.3534
12	0.5397	0.2588	76	0.4846	0.3000
13	0.5352	0.2734	77	0.5133	0.2533
14	0.5299	0.2860	78	0.5988	0.2695
15	0.5250	0.3000	79	0.5543	0.2826
16	0.5214	0.3143	80	0.5607	0.2717
17	0.5177	0.3266	81	0.5583	0.3000
18	0.5155	0.3402	82	0.5600	0.2800
19	0.5114	0.3523	83	0.5625	0.2708
20	0.5039	0.3669	84	0.5714	0.2857
21	0.4994	0.3803	85	0.6111	0.2222
22	0.4949	0.3939	86	0.5933	0.2200
23	0.4916	0.3870	87	0.5714	0.2250
24	0.4867	0.3800	88	0.5525	0.2250
25	0.4842	0.3726	89	0.5340	0.2220
26	0.4805	0.3655	90	0.5152	0.2222
27	0.4766	0.3574	91	0.5000	0.2400
28	0.4730	0.3514	92	0.4833	0.2600
29	0.4727	0.3394	93	0.4636	0.2781
30	0.4681	0.3298	94	0.4478	0.2985
31	0.4696	0.3165	95	0.4354	0.3166
32	0.4682	0.3045	96	0.4412	0.2941
33	0.4769	0.3077	97	0.5122	0.2683
34	0.4704	0.3111	98	0.4235	0.2941
35	0.4713	0.3138	99	0.4545	0.3182
36	0.4857	0.3143	100	0.4237	0.3051
37	0.4741	0.3202	101	0.4348	0.2609
38	0.4750	0.3250	102	0.4286	0.2500
39	0.4753	0.3270	103	0.4384	0.2740
40	0.4764	0.3298	104	0.4483	0.2989
41	0.4783	0.3326	105	0.4624	0.2849
42	0.4889	0.3333	106	0.4457	0.2717
43	0.4821	0.3393	107	0.4405	0.3095
44	0.4824	0.3412	108	0.4500	0.3000
45	0.4817	0.3467	109	0.4573	0.2965
46	0.4821	0.3500	110	0.4640	0.2920
47	0.4846	0.3513	111	0.4741	0.2852
48	0.4857	0.3571	112	0.4825	0.2775
49	0.4867	0.3583	113	0.4900	0.2720
50	0.4828	0.3621	114	0.4958	0.2667
51	0.4886	0.3653	115	0.5100	0.2600
52	0.4897	0.3655	116	0.5133	0.2533
53	0.4828	0.3678	117	0.5250	0.2500
54	0.4860	0.3671	118	0.5300	0.2420
55	0.4829	0.3688	119	0.5389	0.2352
56	0.4767	0.3721	120	0.5450	0.2300
57	0.4795	0.3699	121	0.5533	0.2267
58	0.4801	0.3706	122	0.5615	0.2154
59	0.4881	0.3788	123	0.5714	0.2105
60	0.5000	0.3878	124	0.5750	0.2083
61	0.5051	0.3959	125	0.5873	0.1984
62	0.5124	0.4050	126	0.6611	0.1561
63	0.5080	0.4491	127	0.7308	0.1154

$$f_h = \frac{1}{\sqrt{2}} - f_g.$$

Since $h \geq 1$, the solution to Eq. (A· 1) is obtained as

$$h = 1 + \frac{-b + \sqrt{b^2 - ac}}{a}. \qquad \text{(A· 2)}$$

As the low frequency components in the white noise are swept out to high frequencies to form the blue noise characteristics, the peak height is monotonically increasing with f_g and reaches $h \simeq 1.9$ at $f_g = \frac{1}{\sqrt{2}}$.

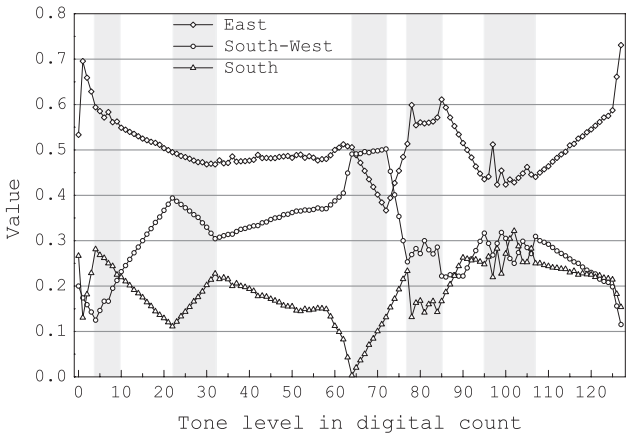

Fig. A· 1 Coefficient values of the error diffusion filters. The shaded and unshaded stripes indicate the intervals specified by a part of extended key levels.

Appendix B: The Optimum Filters

The coefficients of the error diffusion filters optimized for individual 8-bit tones are listed in Table A· 1. They are also plotted in Fig. A· 1 for ease of viewing the variations in the filter coefficients.

Junghyeun Hwang received B.E. and M.E. degrees in electronic engineering from Hoseo University and Dongguk University, Korea, in 1995 and 1997, respectively. Since 2007 he studies at Graduate School of Science and Technology, Niigata University, for Ph.D. His research interests are in the areas of image/video processing including video coding and digital halftoning. He is a Student Member of IEEE.

Hisakazu Kikuchi received B.E. and M.E. degrees from Niigata University, Niigata, in 1974 and 1976, respectively, and Dr.Eng. degree in electrical and electronic engineering from Tokyo Institute of Technology, Tokyo, in 1988. From 1976 to 1979 he worked at Information Processing Systems Lab., Fujitsu Ltd., Tokyo. Since 1979 he has been with Niigata University, where he is a Professor at Department of Electrical and Electronic Engineering. During a year of 1992 to 1993, he was a visiting scholar at Electrical Engineering Department, University of California, Los Angeles, U.S.A. He holds a visiting professorship at Chongqing University of Posts and Telecommunications and Nanjing University of Information Science and Technology, both in China, since 2002 and 2005, respectively. His research interests include digital signal processing and image/video processing. He is a Member of ITE, IIEEJ, and IEEE. He served the chair of Circuits and Systems Group, IEICE, in 2000, the general chair of Digital Signal Processing Symposium, IEICE, in 1988 and Karuizawa Workshop on Circuits and Systems, IEICE, in 1996, respectively, and the technical program chair of ITC-CSCC in 2004.

Shogo Muramatsu received B.E, M.E. and Ph.D. degrees in electrical engineering from Tokyo Metropolitan University in 1993, 1995 and 1998, respectively. From 1997 to 1999, he worked at Tokyo Metropolitan University. In 1999, he joined Niigata University, where he is currently an associate professor of Electrical and Electronics Engineering, Faculty of Engineering. During year from 2003 to 2004, he was a visiting researcher at University of Florence, Italy. His research interests are in digital signal processing, multi-rate systems, video analysis and hardware architecture. He is a member of IEEE and ITE.

Jaeho Shin received the B.E., M.E. and Ph.D. degrees in electronics engineering from Seoul National University, Seoul, Korea, in 1979, 1982 and 1987 respectively. He is a Professor in the Department of Electronic Engineering, Dongguk University in Seoul, Korea. His research interests include digital signal processing, digital system design, and information security. He is a member of IEEE, IEEK, KICS, KISSC, and KISS.